Article

Formation of Formaldehyde and Other Byproducts by TiO₂ Photocatalyst Materials

Weijia Yu [1], **Marten in 't Veld [1,2]**, **Rossana Bossi [2]**, **Mohamed Ateia [3,4]**, **Dominique Tobler [1]**, **Anders Feilberg [5]** and **Nicolas Bovet [1]** and **Matthew S. Johnson [1,*]**

1   Department of Chemistry, University of Copenhagen, Universitetsparken 5, DK-2100 Copenhagen, Denmark; weijia@chem.ku.dk (W.Y.); Marten.Veld@idaea.csic.es (M.i.'tV.); dominique.tobler@chem.ku.dk (D.T.); nbovet@dtu.dk (N.B.)
2   Department of Environmental Science, Aarhus University, Frederiksborgvej 399, DK-4000 Roskilde, Denmark; rbo@envs.au.dk
3   Department of Chemistry, Northwestern University, Evanston, IL 60208, USA; mohamedateia1@gmail.com
4   Department of Environmental Engineering and Earth Science, Clemson University, Clemson, SC 29634, USA
5   Department of Biological and Chemical Engineering, Aarhus University, Nordre Ringgade 1, DK-8000 Aarhus, Denmark; af@bce.au.dk
*   Correspondence: msj@chem.ku.dk; Tel.: +45-40-498-921

Abstract: Photocatalysts promised to control pollution in an environmentally benign manner, inexpensively, and with a low or cheap energy input. However, the limited chemical activity of photocatalysts has prevented their widespread use. This limitation has two important consequences; in addition to limited removal efficiency for pollution, photocatalysts may also generate unwanted byproducts due to incomplete reaction. This study focuses on the byproducts formed in the photocatalytic degradation of dimethyl sulfide (DMS) on titanium dioxide (TiO₂), using a continuous flow reactor and detection via proton transfer reaction mass spectrometry. TiO₂, activated carbon (AC), TiO₂/AC (1:1) and TiO₂/AC (1:5) were tested using either a laser-driven light source or LED lamps at 365 nm. The samples were characterized using a N₂-BET surface area and pore size distributions, Scanning Electron Microscopy, X-ray Diffraction, and X-ray Photoelectron Spectroscopy, which confirmed that TiO₂ was successfully coated on activated carbon without unexpected phases. TiO₂ and activated carbon showed different removal mechanisms for DMS. The maximum yield of formaldehyde, 11.4%, was observed for DMS reacting on a TiO₂/AC (1:5) composite operating at a DMS removal efficiency of 31.7% at 50 °C. In addition to formaldehdye, significant products included acetone and dimethyl disulfide. In all, observed byproducts accounted for over half of the DMS material removed from the airstream. The TiO₂/AC (1:5) and TiO₂/AC (1:1) composites have a lower removal efficiency than TiO₂, but a higher yield of byproducts. Experiments conducted from 20 °C to 70 °C showed that as temperature increases, the removal efficiency decreases and the production of byproducts increases even more. This is attributed both to decreased surface activity at high temperatures due to increased recombination of reactive species, and to the decreased residence time of volatile compounds on a hot surface. This study shows that potentially dangerous byproducts are formed by photocatalytic reactors because the reaction is incomplete under the conditions generally employed.

Keywords: photocatalysts; air pollution control; byproducts; dimethyl sulfide; formaldehyde

1. Introduction

Air pollution is the leading environmental risk factor worldwide, killing an estimated 8.8 million people annually [1], rivaling tobacco smoke and exceeding deaths from all forms of violence combined [1,2]. Exposure to air pollutants increases the risk of respiratory and cardiovascular disease [3]. In addition, there are many associated negative impacts on society, including decreased performance and productivity [4], mental health issues [5], and an increase in violent crime [6]. Humans spend 80 to 90% of their time indoors, bringing increased

attention to indoor air quality [7]. Photocatalysis is promoted as a solution to indoor air quality problems based on assertions regarding its low cost, energy efficiency, and environmentally benign character [8,9]. Photocatalytic oxidation has been studied for its ability to degrade many pollutants, including nitrogen oxides [10,11], sulfur dioxide [12,13], and volatile organic compounds (VOCs) [14–16], which are harmful to human health [3,17]. Photocatalysis could potentially find application in many devices, such as photocatalytic coatings and filters [4]. The efficiency of these materials is the subject of significant research and debate [15,18].

Many studies have been carried out on photocatalytic materials [19]. TiO_2 has been studied the most frequently because it is cheap, non-toxic, biologically inert, and absorbs solar light [20–22]. The photocatalytic activity of TiO_2 depends on its crystalline form. There are three main forms: anatase, rutile, and brookite [23,24]. Anatase is an indirect bandgap semiconductor and has been shown to have better photocatalytic properties than the other two phases, including a longer lifetime for its photoexcited electrons and holes [25]. Anatase can only be stimulated by light with a wavelength shorter than 400 nm [26], which limits its efficiency and applications. Rutile can be activated by visible light (bandgap 3.0 eV; absorbs wavelengths around 400 nm) [27], but because of the rapid recombination of electrons and holes [28], it is not able to maintain a high surface activity as a photocatalyst. Degussa P25 is a photocatalyst composed of anatase and rutile (the reported ratio being typically 70:30 or 80:20) [29–31] which is widely used due to its relatively high photocatalytic activity [32].

Activated carbon (AC) is commonly used for pollution control and works through a mechanism of adsorption rather than photocatalytic degradation. It is inexpensive, stable, and durable, with a large specific surface area and pore volume. The combination of TiO_2 with activated carbon has been studied since the 90s [33–38]. These studies show that the combination of TiO_2 and AC has a higher photocatalytic efficiency than either pure activated carbon or pure TiO_2 [39–41] and improved removal efficiency compared to TiO_2 alone in a high-humidity environment ([42]). Carbon-doped TiO_2 has been shown to respond to visible light, and has higher removal efficiency than undoped TiO_2 [43,44]. Activated carbon may improve TiO_2 photocatalytic degradation by concentrating the pollutants and intermediates for reaction with TiO_2. The pollutants stored in AC can then be destroyed by TiO_2, leading to the regeneration of AC. Finally, the presence of AC limits the coagulation of TiO_2, thus improving its photocatalytic efficiency.

While it is often claimed that by using photocatalysts, VOC pollution will be completely degraded into CO_2 and H_2O [15], this assertion is incomplete and inaccurate. The surface activity of a photocatalyst is self-limiting due to recombination reactions. Only a certain activity can be maintained. An additional concern is that volatile compounds, including volatile reaction products, spend little time on the surface, decreasing the probability of reaction and increasing treatment time. Most studies investigating photocatalytic removal of VOCs calculate the removal efficiency [45–47], or compare the CO_2 production [48–50] of different materials [47,51,52]. For one thing, the treatment times, space velocities, and energy used in these studies are often not practical for applications in the real world. For another, few groups report the yield of CO_2 and H_2O relative to the amount of pollutant consumed. Moreover, monitoring many byproducts including formaldehyde and multiply-oxygenated species requires special techniques that are not always available [53]. A full picture can only be given by considering the mass or atom budgets that describe how much reagent has been lost and which products have been formed, including byproducts.

Although there are studies indicating that photocatalytic oxidation does not completely oxidize organics to CO_2 and H_2O, only a few have examined the byproducts. Selishchev et al. [54] found CO was formed along with CO_2 and H_2O during photocatalytic oxidation of VOCs. Mo et al. [49] found that humidity and VOC concentration affected the formation and concentration of byproducts in a study of the degradation of toluene. Yao and Feilberg observed the formation of methane thiol and S-methyl-methanethiosulfonate from sulfur-containing precursors [55]. Wang and coworkers studied the degradation of DMS on TiO_2, characterizing the products using chromatography, and did not report CH_2O concentrations [56]. Lin et al. saw formaldehyde production from S-doped TiO_2 photocata-

lysts but did not report the yield [57]. Although photocatalysts are studied in the context of indoor air quality, it is essential to characterize byproduct formation in order to conclude that photocatalytic devices are safe and effective. More studies are clearly needed that quantify the yields of CO_2 and H_2O in relation to the loss of precursors, and that account for the transfer of material into byproducts.

In some cases, such as the decomposition of a hydrocarbon-yielding formaldehyde, the products are more dangerous than the original pollutant. Formaldehyde is toxic to humans and animals in small quantities [58]. In 2010, the World Health Organization (WHO) established an indoor air quality guideline for short- and long-term exposure to formaldehyde of 0.1 mg/m^3 (0.08 ppm) for all 30 min periods [59]. The German Federal Agency of Health set a maximum formaldehyde mixing ratio of 0.1 ppm for indoor air, and the US National Institute for Occupational Safety and Health (NIOSH) set a time-weighted average concentration exposure limit for a 10 h workday during a 40 h workweek for formaldehyde of 0.016 ppm [60].

Reduced sulfur compounds are associated with strong odor discomfort and are often a serious pollution problem [61]. They are produced by many processes, such as cooking cabbage, beet, or seafood, by bacteria, and in wastewater treatment. DMS with a very low odor threshold of 0.6–30 ppb [62] is the most abundant biological sulfur compound emitted to the atmosphere. Although its main atmospheric source is marine phytoplankton [63], it is produced by many processes, such as those listed here, and is commonly found in indoor environments. For example, DMS produced by livestock can be the cause of tension between livestock producers and nearby residents. The literature shows that indoor concentrations of DMS are highly variable, ranging from ppt to tens or hundreds of ppb [64,65].

Proton-Transfer-Reaction Mass Spectrometry (PTR-MS) is a powerful method for monitoring byproducts at ppbv levels in real-time that is able to overcome the limited sampling frequency of methods such as gas chromatography-mass spectrometry (GC-MS) [66]. In this work, online PRT-MS was used to monitor the concentrations of DMS and other volatile byproducts.

This study was carried out in order to better characterize the formation of byproducts by common photocatalysts. In particular, we focused on the degradation and byproducts from dimethyl sulfide, important in its own right and as a representative of odorous sulfur compounds in general. Here, we describe the activity, reaction mechanisms, extent of reaction, and yields of several volatile byproducts under typical photocatalyst operating conditions for TiO_2 and composite TiO_2-activated carbon materials, using PTR-MS for accurate and wide-ranging characterisation of reaction products.

2. Results And Discussion

2.1. Characterization

The success of the synthesis and the ratio of the TiO_2/AC was confirmed using SEM, the BET adsorption isotherm method, XPS, and XRD. The details can be found in the electronic Supplementary Materials. Characterizations confirm the successful synthesis of TiO_2/AC (1:1) and TiO_2/AC (1:5), see Supplementary Materials.

2.2. Byproducts

Figure 1 shows the PTR-MS photocatalysis response for experiments testing the TiO_2 photocatalytic removal of DMS. Mass to charge ratios (*m/z*) of 31, 46, 59, 63, and 95 were detected by PTR-MS in full scan mode, assigned to formaldehyde, acetone, formic acid, DMS, and dimethyl disulfide (DMDS), respectively [55]. Those products are probable byproducts of DMS breakdown by ·OH and h^+ [67]. When irradiated with the LDLS lamp, the DMS concentration rapidly decreased by approximately 47.4% and the concentrations of formaldehyde and acetone increased by ca. 20 and 5 ppb, respectively. A minor amount of formic acid was present as an impurity in the gasline, and can be seen in Figure 1. When the lamp was turned on, its concentration also decreased by about 46%. When

the LDLS was turned off, the concentrations of DMS and formic acid increased again, while the concentrations of formaldehyde and acetone showed a clear decrease, which indicates that those products are generated by the photocatalytic process. Blank tests were performed under the following conditions: (1) Blank filter with DMS and LDLS light irradiation, and (2) TiO_2 coated filter with LDLS light irradiation. No byproducts were detected in the blank test.

As shown in Figure 1, during the photocatalytic degradation, the yields of formaldehyde, acetone, DMDS are 5.2%, 1.8% and −0.5%; similar values have been reported in other work, formaldehyde was reported as a byproduct of photocatalytic oxidation of toluene [55,64]. Soni and coworkers have investigated the degradation of DMS on oxidising metal oxide catalyst surfaces and theorize that nucleophilic lattice-stablized $M - O^-$ is responsible for the formation of partial oxidation products [68].
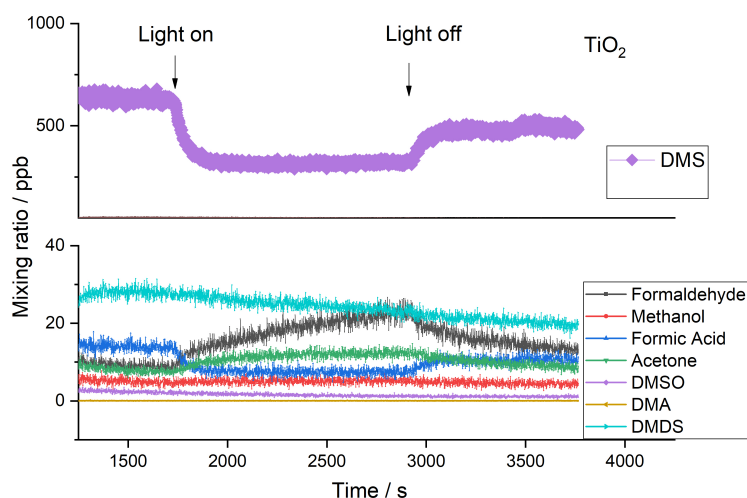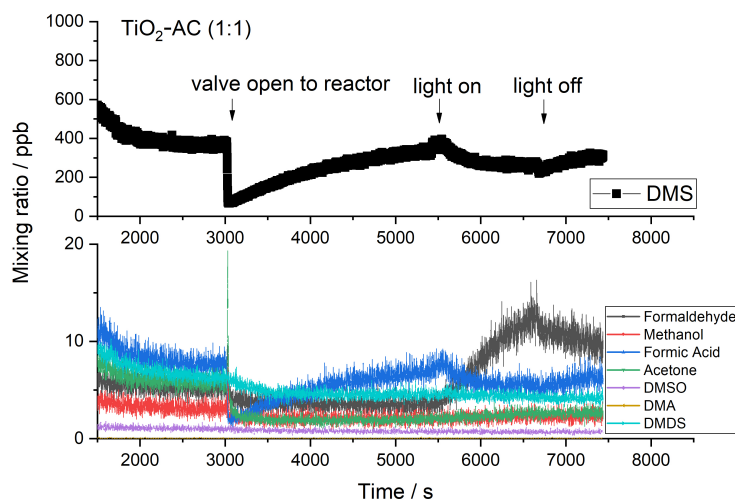

Figure 1. Byproducts of TiO_2 photocatalytic degradation of DMS, with LDLS lamp excitation.

Figure 2 shows the DMS photocatalytic removal efficiency for TiO_2/AC (1:1) photocatalyst excited with the LDLS lamp including DMS byproducts. As shown in Figure 2, the reaction process goes through two phases. Initially, concentrations decrease without byproduct formation, attributed to adsorption on AC. After the AC is saturated, indicated by the return to initial/baseline concentration, the LDLS is turned on and we attribute product formation to TiO_2 photocatalysis. The concentration of DMS decreases by 23%. The decrease in DMS is less than that for pure TiO_2. For this phase, the yields of formaldehyde, acetone, and DMDS are 12.3%, 0.5%, and −0.2%, respectively.

Figure 3 shows the photocatalytic degradation of DMS on TiO_2/AC (1:5) with the LDLS lamp, including byproducts. The behavior is similar as for TiO_2/AC (1:1), though with a longer breakthrough time. The removal efficiency of DMS was 13.4% on TiO_2/AC (1:5). The yields χ of formaldehyde and acetone are 11.2% and 2.4%, respectively, and other intermediates are below the detection limit.

The removal efficiency of DMS and byproduct yield χ are summarized in Table 1. The removal of DMS decreases with a decrease in a TiO_2 mixing ratio in substrates. The adsorption capacity q_e is reported as a mass fraction of adsorbed gas to filter mass [69].
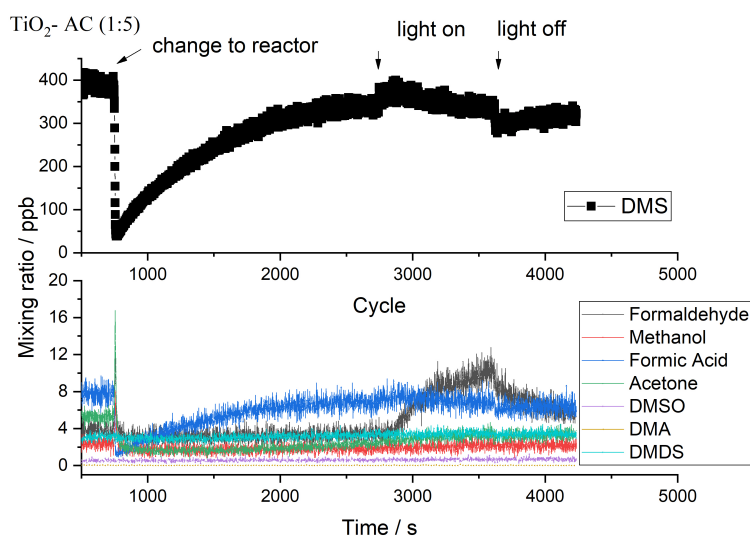
Figure 2. Byproducts of TiO$_2$/AC (1:1) photocatalytic degradation of DMS with LDLS lamp excitation.

Table 1. Summary of the removal efficiencies of DMS f_{RE} for TiO$_2$, TiO$_2$/AC (1:1) and TiO$_2$/AC (1:1) and byproduct yields χ.

Substrate	f_{RE}/%	χ_{CH_3O}/%	$\chi_{CH_3COCH_3}$/%	$\chi_{CH_3SSCH_3}$/%
TiO$_2$	47.4	5.2	0.5	−0.5
TiO$_2$/AC (1:1)	22.9	12.3	0.5	−0.2
TiO$_2$/AC (1:5)	13.4	11.2	0.2	−0.4

The q_e of TiO$_2$/AC (1:1) and TiO$_2$/AC (1:5) are found to be 43.9 mg/g and 46.9 mg/g; the adsorption capacity increases with increasing AC. While the lower TiO$_2$ loading showed lower removal of DMS, it showed a relatively higher yield of byproducts (Table 1).

A scheme for the reactions of organosulfur compounds on TiO$_2$ is presented in Figure 4 [70,71]; the mechanism of acetone formation is unclear.

Figure 3. Byproducts of TiO$_2$/AC (1:5) photocatalytic degradation of DMS with LDLS lamp excitation.
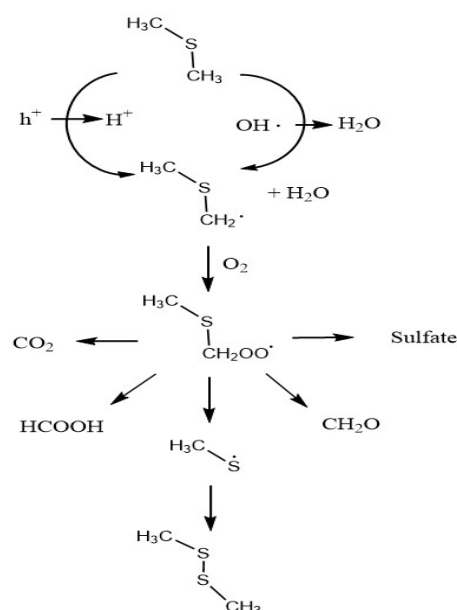
Figure 4. Proposed photocatalytic oxidation pathways of DMS considering direct electron transfer of hole and hydroxyl radical oxidation.

2.3. Influence of Temperature

TiO_2 and AC/TiO_2 (1:1) were chosen for a study of the effect of temperature on catalytic performance and byproduct formation. Conditions were 20 °C, 30 °C, 50 °C, and 70 °C, using the LDLS lamp as the light source.

Figure 5 shows the removal efficiency and byproduct formation for DMS degradation at different temperatures on TiO_2. The concentrations of DMS and DMDS increase with temperature, which can be related to desorption. As summarized in Table 2, when the temperature is elevated from 20 to 70 °C, the RE of DMS decreases from 58.1% to 48.1% and byproduct yield decreases. The highest yield of byproducts is observed at 50 °C with 21.0% for formaldehyde and 15.5% for acetone. In contrast to larger molecules, small molecules spend less time on the surface, and therefore have a lower probability of reaction. Table 3 summarises some key physical properties of these small molecules. Formaldehyde has the lowest vapor pressure, giving less time on the photocatalyst surface. This, combined with a mechanism favoring its production, means that it is one of the most abundant byproducts.

Table 2. The removal efficiency and byproduct yields for DMS with LDLS light excitation on TiO_2 at 20 temperature, 30 °C, 50 °C, and 70 °C.

T/°C	$f_{CH_3SCH_3}$/%	χ_{CH_2O}/%	$\chi_{CH_3COCH_3}$/%	$\chi_{CH_3SSCH_3}$/%
20	58.1	12.8	3.6	5.2
30	50.1	18.1	2.4	8.4
50	49.2	21.0	15.5	5.4
70	48.1	7.4	4.6	12.4

Table 3. Physical properties of product molecules.

Name	Formula	Vapor Pressure	Solubility	Boiling Point	Dipole Moment
Carbon monoxide	CO	>35 atm	2%	−191.5 °C	0.122 D
Carbon dioxide	CO_2	56.5 atm	0.2% (25 °C)	78.48 °C	-
Methane	CH_4	4.7×10^4 kPa (25 °C)	3.5 mL/100 mL at (17 °C)	−161 °C at 101.32 kPa	-
Formaldehyde	CH_2O	1.40 kPa at 25 °C	$4.00 \times 10 + 5$ mg/L at 20 °C	−21 °C at 101.32 kPa	2.330 D
Dimethyl sulfide	CH_3SCH_3	53.7 kPa (at 20 °C)	22 mg/mL at 25 °C	37.2 °C at 101.32 kPa	1.499 D
Acetone	C_3H_6O	9.39 kPa (0 °C) 30.6 kPa (25 °C) 374 kPa (100 °C) 2.8 MPa (200 °C)	Miscible	56.05 °C (44 °C)	2.91 D
Dimethyl disulfide	CH_3SSCH_3	3.8 kPa (at 25 °C)	2.5 g/L (20 °C)	110 °C	1.50 D

* Data were acquired from PubChem (https://pubchem.ncbi.nlm.nih.gov/ accessed on 15 March 2021).
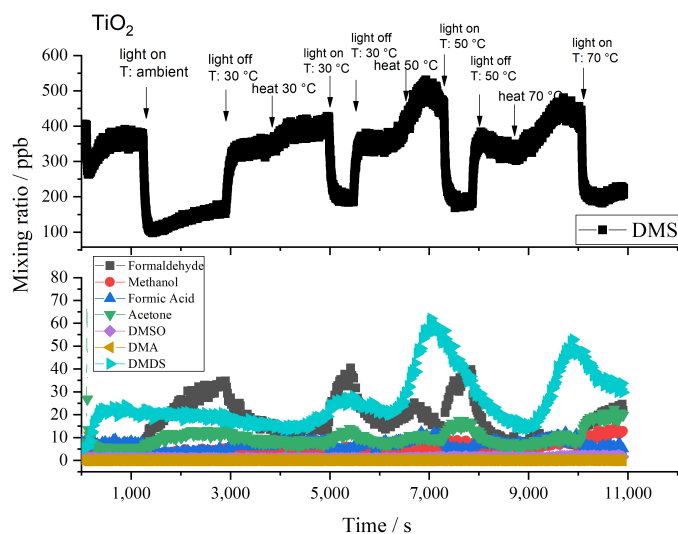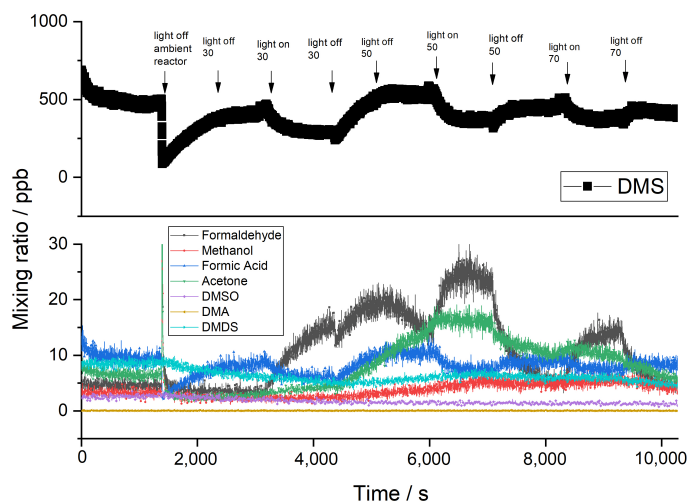

Figure 5. Byproducts of TiO_2 photocatalytic degradation of DMS.

Figure 6 and Table 4 show the removal efficiency and byproduct formation for the degradation DMS on TiO_2/AC (1:1) from 20 to 70 °C. The temperature has a great impact on byproduct formation by TiO_2/AC (1:1) by affecting both the residence time of molecules on the surface and the recombination rate of radicals. Overall, the DMS removal efficiency decreased. Values were 28.2, 32.9, 16, and 11.1% at 20, 30, 50, and 70 °C, respectively. The yield of byproducts was at a maximum of 50 °C with formaldehyde, acetone, and DMDS yields of 32.7%, 21.2%, and 1.0%, respectively. Unlike TiO_2, byproduct generation did not decrease with f for TiO_2/AC (1:1). At 70 °C the yield of formaldehyde decreased to 20.4%. It is worth noting that there is a significant decrease of byproduct yield at 70 °C in both TiO_2 and TiO_2/AC (1:1) experiments. Compared to TiO_2, TiO_2/AC (1:1) has lower f_{DMS} and χ at all temperatures. The results are consistent with a mechanism whereby surface activity decreases at higher temperatures, and in addition, the residence time of volatile byproducts on the surface decreases more rapidly than it does for DMS. The overall effect is decreased pollution removal and more formation of byproducts as temperature increases.

Figure 6. Byproducts of TiO_2/AC (1:1) photocatalytic degradation of DMS by LDLS lamp as a function of temperature.

Table 4. The removal efficiency and byproduct yields for DMS degradation with LDLS light excitation on TiO_2/AC (1:1) at 20, 30, 50, and 70 °C.

$T/°C$	$f_{CH_3SCH_3}/\%$	$\chi_{CH_2O}/\%$	$\chi_{CH_3COCH_3}/\%$	$\chi_{CH_3SSCH_3}/\%$
20	28.2	9.3	1.3	−0.1
30	32.9	8.9	1.6	−0.6
50	16.0	31.7	21.2	1.0
70	11.1	20.4	17.1	1.7

3. Materials And Methods

3.1. Materials

TiO_2 P25 was purchased from Sigma Aldrich, Steinheim, Germany, and AC was purchased from Cica-Reagent, Kanto Chemical Co., Inc., Tokyo, Japan. The TiO_2-AC powders were synthesized by sonicating AC for 1 min in 50 mL of ethanol for each carbonaceous material (solution A). The TiO_2 powder was sonicated in 50 mL of ethanol for 1 min (solution B). Thereafter, solution A and solution B were mixed with mass ratios 1:5 and 1:1, and sonicated for 1 min, followed by mixing for 12 h to produce solution C. After the mixing, solution C was filtered through a vacuum filter machine equipped with a fiberglass filter to separate the product from the supernatant. Afterward, the filter was dried at room temperature for 24 h.

3.2. Methods

The photocatalytic activity of the samples towards dimethyl sulfide (DMS) (Sigma-Aldrich, ≥99%, Steinheim, Germany) under the irradiation of simulated solar light was measured in a continuous flow stainless-steel gas-phase reactor with a quartz window. Samples were irradiated using either a Laser-Driven Light-Source (LDLS, ENERGETIC, 140 W, EQ-99, Wilmington, NC, USA) in combination with a bandpass filter, or with UV light emitting diodes (LED). The LDLS has a spectral distribution similar to the sun. A long-pass filter (335 nm wavelength, Jenaer Glaswerk Schott & Gen., Mainz, Germany) was used to limit irradiation to the region from 335 nm to 2000 nm. Four LED lamps (365–370 nm, 3 W, Hotred, China) were used.

TiO_2, AC, and TiO_2/AC powders were coated on quartz fiber filters (diameter: 47 mm, Whatman, Germany), and the filter was placed in the middle of the reactor (inner diameter: 40 mm, height: 40 mm, cylinder with quartz window). The flow enters from the top of the filter, then leaves from the bottom.

Dry air from a technical air supply was branched into two. One stream flowed through a bubbler with DMS in squalene and the flow from the other adjusted to further control the DMS mixing ratio (Figure 7). The flow rates of the DMS bubbler and the dilution line were controlled by mass flow controllers (Model 0254, Brooks Instruments, Hatfield, PA, USA). The two branch lines were merged at the reactor. The initial concentrations of DMS in the air varied between 300 and 600 ppb. DMS concentrations in the outlet gas mixtures were monitored using PTR-MS (PTR-ToF 8000, Ionicon Analytik GmbH, Innsbruck, Austria). The composition was recorded every second throughout a photolysis experiment. Before irradiation, the air stream with a known concentration of DMS was allowed to flow through the bypass. After the concentrations stabilised, the flow was changed from bypass to reactor until the equilibrium "dark" adsorption of DMS on the samples was established. When the DMS concentrations leaving the reactor were stabilized and equivalent to the concentration before the bypass, the equilibrium was considered to have been reached, and samples would be irradiated by light until the concentration was stable. The removal efficiency f of DMS is given by:

$$f = \frac{C_{in} - C_{out}}{C_{in}},$$ (1)

where C_{in} and C_{out} are the concentrations measured at the inlet and outlet of the reactor, respectively. The yield of byproducts χ is defined as:

$$\chi = \frac{\Delta C_{out}}{\Delta C_{in}}.$$ (2)
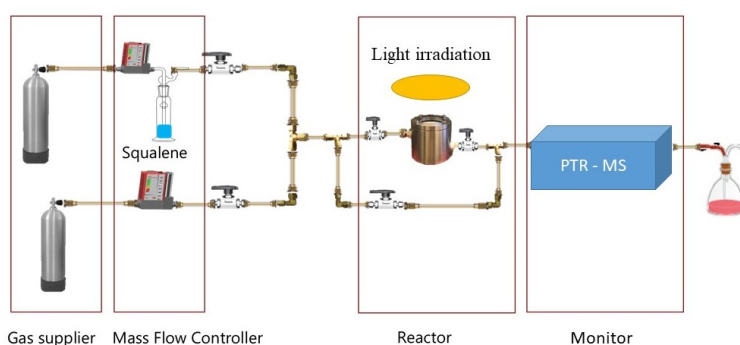
Figure 7. Process diagram of the photocatalytic reaction system setup.

3.3. Characterization

Surface topography was characterised using Scanning Electron Microscopy (SEM, FEI Quanta 3D). The crystal phase and structure of samples were analyzed by X-ray Diffraction (XRD, Bruker D8 Advance Da Vinci). Surface area, total pore volume, and average pore size were analyzed using the BET adsorption isotherm method on a Quantachrome, Autosorb-1. XPS was used to characterize the differences in surface composition. A Kratos AXIS ULTRADLD XPS was used for measurement, and the CasaXPS software was used for data processing. The concentration of gases (in ppbv) was measured by PTR-MS. The PTR-MS samples air continuously into the drift tube where the sample collides with the primary ion H_3O^+, ionizing the compounds via gas phase proton transfer. The proton affinity of water is 691 kJ mol^{-1}, and only compounds with proton affinities above 691 kJ mol^{-1} can be detected by PTR-MS [55].

3.4. Formaldehyde Calibration

The proton affinity of formaldehyde (712.9 kJ/mol) is only 22 kJ/mol higher than the proton affinity of water. Therefore, the formaldehyde signal depends on the humidity [72]), in contrast to most other species detected with PTRMS [73–76]. A formaldehyde calibration based on two parameters (the formaldehyde sensitivity and the humidity) was performed, arriving at the values we have reported. As a formaldehyde permeation sys-

tem was not available, the formaldehyde sensitivity was determined using the method of Wisthaler et al. [77]. In this method, acetaldehyde was used as a surrogate for formaldehyde. Acetaldehyde is a useful surrogate as its chemical and physical properties closely resemble formaldehyde. In their research, Wisthaler et al. calculated that this method added an additional uncertainty of 10% compared to a formaldehyde calibration. Using two different calibration gases, the acetaldehyde (and the formaldehyde) sensitivity of the PTR-MS was set at $101.38667 \pm 0.036\%$ ccps/ppb. With the sensitivity known, the impact of the humidity on the formaldehyde concentrations could be determined. The humidity correction factor (HCF) was calculated by measuring concentrations of formaldehyde in an environmental chamber simultaneously with a PTR-MS and dinitrophenylhydrazine (DNPH) cartridges, which are not affected by humidity [77,78]. The cartridges were analysed using high-performance liquid chromatography with ultraviolet spectroscopy (HPLC-UV). Four measurements were performed in the relative humidity range of 30 to 65%, which showed a linear relationship between the methods [79]:

$$HCF = 0.257 * AH + 3.6722, \qquad (3)$$

where AH is the absolute humidity in gm^{-3}. Finally, the formaldehyde concentrations were determined using the following formula:

$$HCHO_{ppb} = \frac{HCHO_{ccps}}{101.38667} * (0.257 * AH + 3.6722), \qquad (4)$$

where $HCHO_{ppb}$ is the formaldehyde concentration in the ppb level, and $HCHO_{ccps}$ is the signal of formaldehyde in corrected counts per second.

4. Conclusions

TiO_2, TiO_2/AC (1:1), and TiO_2/AC (1:5) samples were tested for DMS removal. While under LDLS irradiation, the main byproducts generated by TiO_2 were formaldehyde and acetone. The byproduct yield increased with TiO_2 loading. For TiO_2, DMS removal efficiency decreased, and byproduct yield increased as a function of temperature. TiO_2/AC (1:1) performed differently than TiO_2 since AC is able to release stored pollutants with increasing temperature. At a higher temperature, the f_{DMS} of TiO_2/AC (1:1) decreased, and the byproduct yield increased. The most common byproduct is formaldehyde, which reached a maximum yield of 31.7% at 50 °C on TiO_2/AC (1:1) substrate. We conclude that surface activity decreases at a higher temperature due to increased loss of radicals to recombination reactions, and in addition, the residence time of volatile byproducts on the surface decreases more rapidly than it does for DMS. The overall effect is decreased pollution removal and more formation of byproducts as temperature increases. None of the substrates was capable of fully degrading DMS into CO_2 and H_2O under the conditions of the study. At higher temperatures, both DMS and intermediates spend less time on the surface, limiting their removal; at the same time, surface activity drops as temperature increases due to increased loss of radicals. In conclusion, care must be taken to include consideration of byproduct formation when evaluating the performance of photocatalysts, particularly for indoor applications where there is potential for accumulation of toxic products.

Author Contributions: Conceptualization, W.Y. and M.S.J.; Methodology, W.Y. and M.S.J.; Software, M.i.'tV., D.T.; Validation, W.Y. and M.S.J.; Formal analysis, W.Y. and M.S.J.; Investigation, W.Y., M.i.'tV.; Resources, D.T., R.B., A.F., M.A. and N.B.; Data curation, W.Y.; Writing—original draft preparation, W.Y.; Writing—review and editing, M.S.J.; Visualization, W.Y.; Supervision, M.S.J.; Project administration, M.S.J.; Funding acquisition, W.Y. and M.S.J. All authors have read and agreed to the published version of the manuscript.

References

1. Lelieveld, J.; Pozzer, A.; Pöschl, U.; Fnais, M.; Haines, A.; Münzel, T. Loss of life expectancy from air pollution compared to other risk factors: A worldwide perspective. *Cardiovasc. Res.* **2020**, *116*, 1910–1917. [CrossRef]
2. Landrigan, P.J.; Fuller, R.; Acosta, N.J.; Adeyi, O.; Arnold, R.; Baldé, A.B.; Bertollini, R.; Bose-O'Reilly, S.; Boufford, J.I.; Breysse, P.N.; et al. The Lancet Commission on pollution and health. *Lancet* **2018**, *391*, 462–512. [CrossRef]
3. Brunekreef, B.; Holgate, S.T. Air pollution and health. *Lancet* **2002**, *360*, 1233–1242. [CrossRef]
4. Wyon, D.P. The effects of indoor air quality on performance and productivity. *Indoor Air* **2004**, *14*, 92–101. [CrossRef] [PubMed]
5. Chen, S.; Oliva, P.; Zhang, P. *Air Pollution and Mental Health: Evidence from China*; Technical Report; National Bureau of Economic Research: Cambridge, MA, USA, 2018.
6. Burkhardt, J.; Bayham, J.; Wilson, A.; Berman, J.D.; O'Dell, K.; Ford, B.; Fischer, E.V.; Pierce, J.R. The relationship between monthly air pollution and violent crime across the United States. *J. Environ. Econ. Policy* **2020**, *9*, 188–205. [CrossRef]
7. Saini, J.; Dutta, M.; Marques, G. A comprehensive review on indoor air quality monitoring systems for enhanced public health. *Sustain. Environ. Res.* **2020**, *30*, 6. [CrossRef]
8. Beeldens, A. An environmental friendly solution for air purification and self-cleaning effect: The application of TiO_2 as photocatalyst in concrete. In Proceedings of the Transport Research Arena Europe—TRA, Göteborg, Sweden, 12–15 June 2006; pp. 12–16.
9. Asahi, R.; Morikawa, T.; Ohwaki, T.; Aoki, K.; Taga, Y. Visible-light photocatalysis in nitrogen-doped titanium oxides. *Science* **2001**, *293*, 269–271. [CrossRef] [PubMed]
10. Maggos, T.; Bartzis, J.; Liakou, M.; Gobin, C. Photocatalytic degradation of NOx gases using TiO_2-containing paint: A real scale study. *J. Hazard. Mater.* **2007**, *146*, 668–673. [CrossRef] [PubMed]
11. Maggos, T.; Plassais, A.; Bartzis, J.; Vasilakos, C.; Moussiopoulos, N.; Bonafous, L. Photocatalytic degradation of NOx in a pilot street canyon configuration using TiO_2-mortar panels. *Environ. Monit. Assess.* **2008**, *136*, 35–44. [CrossRef]
12. Yuan, Y.; Zhang, J.; Li, H.; Li, Y.; Zhao, Y.; Zheng, C. Simultaneous removal of SO_2, NO and mercury using TiO_2-aluminum silicate fiber by photocatalysis. *Chem. Eng. J.* **2012**, *192*, 21–28. [CrossRef]
13. Liu, H.; Yu, X.; Yang, H. The integrated photocatalytic removal of SO_2 and NO using Cu doped titanium dioxide supported by multi-walled carbon nanotubes. *Chem. Eng. J.* **2014**, *243*, 465–472. [CrossRef]
14. Alberici, R.M.; Jardim, W.F. Photocatalytic destruction of VOCs in the gas-phase using titanium dioxide. *Appl. Catal. B Environ.* **1997**, *14*, 55–68. [CrossRef]
15. Mo, J.; Zhang, Y.; Xu, Q.; Lamson, J.J.; Zhao, R. Photocatalytic purification of volatile organic compounds in indoor air: A literature review. *Atmos. Environ.* **2009**, *43*, 2229–2246. [CrossRef]
16. Kim, S.B.; Hong, S.C. Kinetic study for photocatalytic degradation of volatile organic compounds in air using thin film TiO_2 photocatalyst. *Appl. Catal. B Environ.* **2002**, *35*, 305–315. [CrossRef]
17. Xu, T.; Zheng, H.; Zhang, P. Performance of an innovative VUV-PCO purifier with nanoporous TiO_2 film for simultaneous elimination of VOCs and by-product ozone in indoor air. *Build. Environ.* **2018**, *142*, 379–387. [CrossRef]
18. Ren, H.; Koshy, P.; Chen, W.F.; Qi, S.; Sorrell, C.C. Photocatalytic materials and technologies for air purification. *J. Hazard. Mater.* **2017**, *325*, 340–366. [CrossRef]
19. Di Paola, A.; García-López, E.; Marcì, G.; Palmisano, L. A survey of photocatalytic materials for environmental remediation. *J. Hazard. Mater.* **2012**, *211*, 3–29. [CrossRef] [PubMed]
20. Palanisamy, B.; Babu, C.; Sundaravel, B.; Anandan, S.; Murugesan, V. Sol–gel synthesis of mesoporous mixed Fe_2O_3/TiO_2 photocatalyst: Application for degradation of 4-chlorophenol. *J. Hazard. Mater.* **2013**, *252*, 233–242. [CrossRef] [PubMed]
21. Fujishima, A.; Honda, K. Electrochemical photolysis of water at a semiconductor electrode. *Nature* **1972**, *238*, 37–38. [CrossRef]
22. Linsebigler, A.L.; Lu, G.; Yates, J.T., Jr. Photocatalysis on TiO_2 surfaces: Principles, mechanisms, and selected results. *Chem. Rev.* **1995**, *95*, 735–758. [CrossRef]
23. Xu, M.; Shao, S.; Gao, B.; Lv, J.; Li, Q.; Wang, Y.; Wang, H.; Zhang, L.; Ma, Y. Anatase (101)-like structural model revealed for metastable rutile TiO_2 (011) surface. *ACS Appl. Mater. Interfaces* **2017**, *9*, 7891–7896. [CrossRef] [PubMed]
24. Yu, J.; Yu, H.; Cheng, B.; Zhou, M.; Zhao, X. Enhanced photocatalytic activity of TiO_2 powder (P25) by hydrothermal treatment. *J. Mol. Catal. A Chem.* **2006**, *253*, 112–118. [CrossRef]
25. Zhang, X.; Zhou, M.; Lei, L. TiO_2 photocatalyst deposition by MOCVD on activated carbon. *Carbon* **2006**, *44*, 325–333. [CrossRef]

26. Sun, Q.; Lv, K.; Zhang, Z.; Li, M.; Li, B.; others. Effect of contact interface between TiO_2 and g-C3N4 on the photoreactivity of g-C$_3$N$_4$/TiO_2 photocatalyst: (0 0 1) vs. (1 0 1) facets of TiO_2. *Appl. Catal. B Environ.* **2015**, *164*, 420–427.

27. Ohno, T.; Tsubota, T.; Toyofuku, M.; Inaba, R. Photocatalytic activity of a TiO_2 photocatalyst doped with C_4^+ and $S4^+$ ions having a rutile phase under visible light. *Catal. Lett.* **2004**, *98*, 255–258. [CrossRef]

28. Zhang, J.; Zhou, P.; Liu, J.; Yu, J. New understanding of the difference of photocatalytic activity among anatase, rutile and brookite TiO_2. *Phys. Chem. Chem. Phys.* **2014**, *16*, 20382–20386. [CrossRef]

29. Ohtani, B.; Prieto-Mahaney, O.; Li, D.; Abe, R. What is Degussa (Evonik) P25? Crystalline composition analysis, reconstruction from isolated pure particles and photocatalytic activity test. *J. Photochem. Photobiol. A Chem.* **2010**, *216*, 179–182. [CrossRef]

30. Hurum, D.C.; Agrios, A.G.; Gray, K.A.; Rajh, T.; Thurnauer, M.C. Explaining the enhanced photocatalytic activity of Degussa P25 mixed-phase TiO_2 using EPR. *J. Phys. Chem. B* **2003**, *107*, 4545–4549. [CrossRef]

31. Ohno, T.; Sarukawa, K.; Tokieda, K.; Matsumura, M. Morphology of a TiO_2 photocatalyst (Degussa, P-25) consisting of anatase and rutile crystalline phases. *J. Catal.* **2001**, *203*, 82–86. [CrossRef]

32. Quesada-Cabrera, R.; Mills, A.; O'Rourke, C. Action spectra of P25 TiO_2 and a visible light absorbing, carbon-modified titania in the photocatalytic degradation of stearic acid. *Appl. Catal. B Environ.* **2014**, *150*, 338–344. [CrossRef]

33. Torimoto, T.; Okawa, Y.; Takeda, N.; Yoneyama, H. Effect of activated carbon content in TiO_2-loaded activated carbon on photodegradation behaviors of dichloromethane. *J. Photochem. Photobiol. A Chem.* **1997**, *103*, 153–157. [CrossRef]

34. Heu, R.; Ateia, M.; Awfa, D.; Punyapalakul, P.; Yoshimura, C. Photocatalytic Degradation of Organic Micropollutants in Water by Zr-MOF/GO Composites. *J. Compos. Sci.* **2020**, *4*, 54. [CrossRef]

35. Ateia, M.; Alalm, M.G.; Awfa, D.; Johnson, M.S.; Yoshimura, C. Modeling the degradation and disinfection of water pollutants by photocatalysts and composites: A critical review. *Sci. Total Environ.* **2020**, *698*, 134197. [CrossRef]

36. Awfa, D.; Ateia, M.; Fujii, M.; Johnson, M.S.; Yoshimura, C. Photodegradation of pharmaceuticals and personal care products in water treatment using carbonaceous-TiO_2 composites: A critical review of recent literature. *Water Res.* **2018**, *142*, 26–45. [CrossRef]

37. Awfa, D.; Ateia, M.; Fujii, M.; Yoshimura, C. Novel magnetic carbon nanotube-TiO_2 composites for solar light photocatalytic degradation of pharmaceuticals in the presence of natural organic matter. *J. Water Process. Eng.* **2019**, *31*, 100836. [CrossRef]

38. Shimizu, Y.; Ateia, M.; Wang, M.; Awfa, D.; Yoshimura, C. Disinfection mechanism of E. coli by CNT-TiO_2 composites: Photocatalytic inactivation vs. physical separation. *Chemosphere* **2019**, *235*, 1041–1049. [CrossRef] [PubMed]

39. Takeda, N.; Iwata, N.; Torimoto, T.; Yoneyama, H. Influence of carbon black as an adsorbent used in TiO_2 photocatalyst films on photodegradation behaviors of propyzamide. *J. Catal.* **1998**, *177*, 240–246. [CrossRef]

40. Ibusuki, T.; Takeuchi, K. Removal of low concentration nitrogen oxides through photoassisted heterogeneous catalysis. *J. Mol. Catal.* **1994**, *88*, 93–102. [CrossRef]

41. Xu, Y.; Langford, C.H. Photoactivity of titanium dioxide supported on MCM41, zeolite X, and zeolite Y. *J. Phys. Chem. B* **1997**, *101*, 3115–3121. [CrossRef]

42. Ao, C.; Lee, S. Combination effect of activated carbon with TiO_2 for the photodegradation of binary pollutants at typical indoor air level. *J. Photochem. Photobiol. A Chem.* **2004**, *161*, 131–140. [CrossRef]

43. Irie, H.; Watanabe, Y.; Hashimoto, K. Carbon-doped anatase TiO_2 powders as a visible-light sensitive photocatalyst. *Chem. Lett.* **2003**, *32*, 772–773. [CrossRef]

44. Chatterjee, A.; Wu, S.B.; Chou, P.W.; Wong, M.; Cheng, C.L. Observation of carbon-facilitated phase transformation of titanium dioxide forming mixed-phase titania by confocal Raman microscopy. *J. Raman Spectrosc.* **2011**, *42*, 1075–1080. [CrossRef]

45. Fang, J.; Chen, Z.; Zheng, Q.; Li, D. Photocatalytic decomposition of benzene enhanced by the heating effect of light: Improving solar energy utilization with photothermocatalytic synergy. *Catal. Sci. Technol.* **2017**, *7*, 3303–3311. [CrossRef]

46. Wang, L.; Zhang, Y.; Gu, X.; Zhang, Y.; Su, H. Insight into the role of UV-irradiation in photothermal catalytic Fischer–Tropsch synthesis over TiO_2 nanotube-supported cobalt nanoparticles. *Catal. Sci. Technol.* **2018**, *8*, 601–610. [CrossRef]

47. Zeng, M.; Li, Y.; Mao, M.; Bai, J.; Ren, L.; Zhao, X. Synergetic effect between photocatalysis on TiO_2 and thermocatalysis on CeO_2 for gas-phase oxidation of benzene on TiO_2/CeO_2 nanocomposites. *ACS Catal.* **2015**, *5*, 3278–3286. [CrossRef]

48. Lan, L.; Li, Y.; Zeng, M.; Mao, M.; Ren, L.; Yang, Y.; Liu, H.; Yun, L.; Zhao, X. Efficient UV–vis-infrared light-driven catalytic abatement of benzene on amorphous manganese oxide supported on anatase TiO_2 nanosheet with dominant {001} facets promoted by a photothermocatalytic synergetic effect. *Appl. Catal. B Environ.* **2017**, *203*, 494–504. [CrossRef]

49. Zheng, Y.; Wang, W.; Jiang, D.; Zhang, L. Amorphous MnOx modified Co$_3$O$_4$ for formaldehyde oxidation: Improved low-temperature catalytic and photothermocatalytic activity. *Chem. Eng. J.* **2016**, *284*, 21–27. [CrossRef]

50. Chen, J.; Li, Y.; Fang, S.; Yang, Y.; Zhao, X. UV–Vis-infrared light-driven thermocatalytic abatement of benzene on Fe doped OMS-2 nanorods enhanced by a novel photoactivation. *Chem. Eng. J.* **2018**, *332*, 205–215. [CrossRef]

51. Ji, J.; Xu, Y.; Huang, H.; He, M.; Liu, S.; Liu, G.; Xie, R.; Feng, Q.; Shu, Y.; Zhan, Y.; et al. Mesoporous TiO_2 under VUV irradiation: Enhanced photocatalytic oxidation for VOCs degradation at room temperature. *Chem. Eng. J.* **2017**, *327*, 490–499. [CrossRef]

52. Fang, S.; Li, Y.; Yang, Y.; Chen, J.; Liu, H.; Zhao, X. Mg-doped OMS-2 nanorods: A highly efficient catalyst for purification of volatile organic compounds with full solar spectrum irradiation. *Environ. Sci. Nano* **2017**, *4*, 1798–1807. [CrossRef]

53. Russell, H.S.; Bonomaully, J.; Bossi, R.; Hofmann, M.E.; Knap, H.C.; Pernov, J.B.; Veld, M.; Johnson, M.S. Novel Materials for Combined Nitrogen Dioxide and Formaldehyde Pollution Control under Ambient Conditions. *Catalysts* **2020**, *10*, 1040. [CrossRef]

54. Selishchev, D.; Kolobov, N.; Pershin, A.; Kozlov, D. TiO$_2$ mediated photocatalytic oxidation of volatile organic compounds: Formation of CO as a harmful by-product. *Appl. Catal. B Environ.* **2017**, *200*, 503–513. [CrossRef]
55. Yao, H.; Feilberg, A. Characterisation of photocatalytic degradation of odorous compounds associated with livestock facilities by means of PTR-MS. *Chem. Eng. J.* **2015**, *277*, 341–351. [CrossRef]
56. Wang, Z.; Liu, J.; Dai, Y.; Dong, W.; Zhang, S.; Chen, J. Dimethyl sulfide photocatalytic degradation in a light-emitting-diode continuous reactor: Kinetic and mechanistic study. *Ind. Eng. Chem. Res.* **2011**, *50*, 7977–7984. [CrossRef]
57. Lin, Y.H.; Hsueh, H.T.; Chang, C.W.; Chu, H. The visible light-driven photodegradation of dimethyl sulfide on S-doped TiO$_2$: Characterization, kinetics, and reaction pathways. *Appl. Catal. B Environ.* **2016**, *199*, 1–10. [CrossRef]
58. Li, Y.; Chen, N.; Deng, D.; Xing, X.; Xiao, X.; Wang, Y. Formaldehyde detection: SnO$_2$ microspheres for formaldehyde gas sensor with high sensitivity, fast response/recovery and good selectivity. *Sens. Actuators B Chem.* **2017**, *238*, 264–273. [CrossRef]
59. Nielsen, G.D.; Larsen, S.T.; Wolkoff, P. Re-evaluation of the WHO (2010) formaldehyde indoor air quality guideline for cancer risk assessment. *Arch. Toxicol.* **2017**, *91*, 35–61. [CrossRef] [PubMed]
60. Nie, L.; Yu, J.; Jaroniec, M.; Tao, F.F. Room-temperature catalytic oxidation of formaldehyde on catalysts. *Catal. Sci. Technol.* **2016**, *6*, 3649–3669. [CrossRef]
61. Cho, K.S.; Hirai, M.; Shoda, M. Degradation characteristics of hydrogen sulfide, methanethiol, dimethyl sulfide and dimethyl disulfide by Thiobacillus thioparus DW44 isolated from peat biofilter. *J. Ferment. Bioeng.* **1991**, *71*, 384–389. [CrossRef]
62. De Zwart, J.M.; Kuenen, J.G. C 1-cycle of sulfur compounds. *Biodegradation* **1992**, *3*, 37–59. [CrossRef]
63. Charlson, R.J.; Lovelock, J.E.; Andreae, M.O.; Warren, S.G. Oceanic phytoplankton, atmospheric sulphur, cloud albedo and climate. *Nature* **1987**, *326*, 655–661. [CrossRef]
64. Zhao, W.; Dai, J.; Liu, F.; Bao, J.; Wang, Y.; Yang, Y.; Yang, Y.; Zhao, D. Photocatalytic oxidation of indoor toluene: Process risk analysis and influence of relative humidity, photocatalysts, and VUV irradiation. *Sci. Total Environ.* **2012**, *438*, 201–209. [CrossRef]
65. Vildozo, D.; Portela, R.; Ferronato, C.; Chovelon, J.M. Photocatalytic oxidation of 2-propanol/toluene binary mixtures at indoor air concentration levels. *Appl. Catal. B Environ.* **2011**, *107*, 347–354. [CrossRef]
66. Irokawa, Y.; Morikawa, T.; Aoki, K.; Kosaka, S.; Ohwaki, T.; Taga, Y. Photodegradation of toluene over TiO$_2$- X N X under visible light irradiation. *Phys. Chem. Chem. Phys.* **2006**, *8*, 1116–1121. [CrossRef] [PubMed]
67. Cantau, C.; Larribau, S.; Pigot, T.; Simon, M.; Maurette, M.; Lacombe, S. Oxidation of nauseous sulfur compounds by photocatalysis or photosensitization. *Catal. Today* **2007**, *122*, 27–38. [CrossRef]
68. Soni, K.C.; Shekar, S.C.; Singh, B.; Gopi, T. Catalytic activity of Fe/ZrO$_2$ nanoparticles for dimethyl sulfide oxidation. *J. Colloid Interface Sci.* **2015**, *446*, 226–236. [CrossRef]
69. Chen, J.; Qin, Y.; Chen, Z.; Yang, Z.; Yang, W.; Wang, Y. Gas circulating fluidized beds photocatalytic regeneration of I-TiO$_2$ modified activated carbons saturated with toluene. *Chem. Eng. J.* **2016**, *293*, 281–290. [CrossRef]
70. Demeestere, K.; Dewulf, J.; De Witte, B.; Van Langenhove, H. Titanium dioxide mediated heterogeneous photocatalytic degradation of gaseous dimethyl sulfide: Parameter study and reaction pathways. *Appl. Catal. B Environ.* **2005**, *60*, 93–106. [CrossRef]
71. Yu, X.; Yin, H.; Ye, J.S.; Peng, H.; Lu, G.; Dang, Z. Degradation of tris-(2-chloroisopropyl) phosphate via UV/TiO$_2$ photocatalysis: Kinetic, pathway, and security risk assessment of degradation intermediates using proteomic analyses. *Chem. Eng. J.* **2019**, *374*, 263–273. [CrossRef]
72. Manheim, J.M.; Milton, J.R.; Zhang, Y.; Kenttamaa, H.I. Fragmentation of saturated hydrocarbons upon atmospheric pressure chemical ionization is caused by proton-transfer reactions. *Anal. Chem.* **2020**, *92*, 8883–8892. [CrossRef] [PubMed]
73. Vlasenko, A.; Macdonald, A.; Sjostedt, S.; Abbatt, J. Formaldehyde measurements by Proton transfer reaction–Mass Spectrometry (PTR-MS): Correction for humidity effects. *Atmos. Meas. Tech.* **2010**, *3*, 1055–1062. [CrossRef]
74. Inomata, S.; Tanimoto, H.; Kameyama, S.; Tsunogai, U.; Irie, H.; Kanaya, Y.; Wang, Z. Determination of formaldehyde mixing ratios in air with PTR-MS: Laboratory experiments and field measurements. *Atmos. Chem. Phys.* **2008**, *8*, 273–284. [CrossRef]
75. Jobson, B.; McCoskey, J. Sample drying to improve HCHO measurements by PTR-MS instruments: Laboratory and field measurements. *Atmos. Chem. Phys.* **2010**, *10*, 1821–1835. [CrossRef]
76. Warneke, C.; Veres, P.; Holloway, J.; Stutz, J.; Tsai, C.; Alvarez, S.; Rappenglueck, B.; Fehsenfeld, F.; Graus, M.; Gilman, J.; et al. Airborne formaldehyde measurements using PTR-MS: Calibration, humidity dependence, inter-comparison and initial results. *Atmos. Meas. Tech.* **2011**, *4*, 2345–2358. [CrossRef]
77. Wisthaler, A.; Apel, E.; Bossmeyer, J.; Hansel, A.; Junkermann, W.; Koppmann, R.; Meier, R.; Müller, K.; Solomon, S.; Steinbrecher, R.; et al. Intercomparison of formaldehyde measurements at the atmosphere simulation chamber SAPHIR. *Atmos. Chem. Phys.* **2008**, *8*, 2189–2200. [CrossRef]
78. Salthammer, T.; Mentese, S. Comparison of analytical techniques for the determination of aldehydes in test chambers. *Chemosphere* **2008**, *73*, 1351–1356. [CrossRef] [PubMed]
79. Cui, L.; Zhang, Z.; Huang, Y.; Lee, S.C.; Blake, D.R.; Ho, K.F.; Wang, B.; Gao, Y.; Wang, X.M.; Louie, P.K.K. Measuring OVOCs and VOCs by PTR-MS in an urban roadside microenvironment of Hong Kong: Relative humidity and temperature dependence, and field intercomparisons. *Atmos. Meas. Tech.* **2016**, *9*, 5763–5779. [CrossRef]